EnM
ENDOCRINOLOGY AND METABOLISM

Original Article

Endocrinol Metab 2023;38:226-244
https://doi.org/10.3803/EnM.2022.1604
pISSN 2093-596X · eISSN 2093-5978

Inhibition of Fatty Acid β-Oxidation by Fatty Acid Binding Protein 4 Induces Ferroptosis in HK2 Cells Under High Glucose Conditions

Jiasi Chen[1,*], Keping Wu[1,2,*], Yan Lei[1,*], Mingcheng Huang[1], Lokyu Cheng[1], Hui Guan[1], Jiawen Lin[1], Ming Zhong[1], Xiaohua Wang[1], Zhihua Zheng[1]

[1]Department of Nephrology, Kidney and Urology Center, The Seventh Affiliated Hospital, Sun Yat-sen University; [2]Renal Division, Peking University Shenzhen Hospital, Shenzhen, China

Background: Ferroptosis, which is caused by an iron-dependent accumulation of lipid hydroperoxides, is a type of cell death linked to diabetic kidney disease (DKD). Previous research has shown that fatty acid binding protein 4 (FABP4) is involved in the regulation of ferroptosis in diabetic retinopathy. The present study was constructed to explore the role of FABP4 in the regulation of ferroptosis in DKD.
Methods: We first detected the expression of FABP4 and proteins related to ferroptosis in renal biopsies of patients with DKD. Then, we used a FABP4 inhibitor and small interfering RNA to investigate the role of FABP4 in ferroptosis induced by high glucose in human renal proximal tubular epithelial (HG-HK2) cells.
Results: In kidney biopsies of DKD patients, the expression of FABP4 was elevated, whereas carnitine palmitoyltransferase-1A (CPT1A), glutathione peroxidase 4, ferritin heavy chain, and ferritin light chain showed reduced expression. In HG-HK2 cells, the induction of ferroptosis was accompanied by an increase in FABP4. Inhibition of FABP4 in HG-HK2 cells changed the redox state, suppressing the production of reactive oxygen species, ferrous iron (Fe^{2+}), and malondialdehyde, increasing superoxide dismutase, and reversing ferroptosis-associated mitochondrial damage. The inhibition of FABP4 also increased the expression of CPT1A, reversed lipid deposition, and restored impaired fatty acid β-oxidation. In addition, the inhibition of CPT1A could induce ferroptosis in HK2 cells.
Conclusion: Our results suggest that FABP4 mediates ferroptosis in HG-HK2 cells by inhibiting fatty acid β-oxidation.

Keywords: Diabetic kidney disease; Ferroptosis; FABP4 protein, human; Fatty acid β-oxidation; Lipid accumulation; Reactive oxygen species

INTRODUCTION

Diabetic kidney disease (DKD) is a major complication of diabetes and the most prevalent cause of end-stage renal disease (ESRD). The prevalence of DKD is on the rise, as about 30% of patients with type 1 diabetes mellitus and 40% of patients with type 2 diabetes mellitus develop DKD [1]. In addition, the percentage of patients with ESRD caused by diabetes increased

Received: 7 October 2022, **Revised:** 15 December 2022,
Accepted: 18 January 2023

Corresponding author: Zhihua Zheng
Department of Nephrology, Kidney and Urology Center, The Seventh Affiliated Hospital of Sun Yat-sen University, No.628, Zhenyuan Road, Guangming District, Shenzhen 518107, China
Tel: +86-755-81206913, **Fax:** +86-755-81206900
E-mail: zhzhihua@mail.sysu.edu.cn

*These authors contributed equally to this work.

from 22.1% in 2000 to 31.3% in 2015 worldwide [2]. Compared to individuals who only have diabetes, patients with both diabetes and DKD have a mortality risk that is 3- to 12-fold higher, and 90% of DKD patients die before progressing to ESRD [3]. Therefore, it is crucial to unravel the underlying pathogenesis of DKD and develop therapeutic strategies.

Ferroptosis is a recently discovered type of programmed cell death that is linked to the pathogenesis of various diseases [4-6]. Ferroptosis is characterized by iron overload, the accumulation of lethal lipid hydroperoxides, a weakened antioxidant capacity, and mitochondrial changes such as smaller mitochondria, diminished or absent mitochondrial cristae, and ruptured mitochondrial outer membranes [7,8]. These manifestations are distinct from those of apoptosis, necroptosis, and pyroptosis [9]. In ferroptosis, lipid peroxidation is caused by reactive oxygen species (ROS) derived from the Fenton reaction, and the accumulation of these peroxides on cellular membranes can damage the membranes and cause cell death [10]. In addition, lipid peroxidation end-products, such as malondialdehyde (MDA), may form toxic adducts with proteins and DNA, leading to significant cytotoxicity and inducing ferroptosis [11]. Physiologically, lipid hydroperoxides are reduced to hydroxy derivatives by glutathione peroxidase 4 (GPX4) and glutathione (GSH), but during ferroptosis, GSH production is reduced, and GPX4 is unable to exert its normal antioxidant capacity due to the disruption of X_c^- transporter [12]. Moreover, ferritin is also involved in the suppression of ferroptosis by storing iron ions [13,14]. Ferritin consists of a heavy chain (FTH) and a light chain (FTL). FTH mediates the conversion of ferrous iron (Fe^{2+}) to the ferric form (Fe^{3+}), which is stored in FTL [15]. Recent evidence points to the role of ferroptosis in the pathology of diverse kidney diseases [16]; specifically, it has been linked to DKD, although the mechanism is not clear [17].

Ferroptosis is regulated by multiple metabolic pathways [18,19]. For example, lipid metabolism pathways can modulate the sensitivity of ferroptosis in various diseases [20,21]. Previous studies have found that a reduction in fatty acid β-oxidation (FAO) increased the susceptibility of renal cell carcinomas to ferroptosis [22]. Typically, mitochondrial FAO consumes most of the fatty acids and reduces lipid peroxidation [23]. However, FAO is reduced in renal carcinomas, increasing their susceptibility to ferroptosis [22]. In patients with diabetes, dyslipidemia is a risk factor for the progression of DKD [24,25]. Abnormal lipid deposition and lipid droplets in glomeruli and tubules were caused by the downregulation of genes for lipolysis and FAO [26,27]. However, it remains unclear whether impaired FAO and lipid accumulation can cause progression to DKD by increasing ferroptosis.

Fatty acid binding protein 4 (FABP4) plays a vital role in lipid metabolism and oxidative stress and contributes to the pathogenesis of a wide variety of metabolic diseases [28,29]. Recent studies have shown that the upregulation of *FABP4* promoted the progression of kidney disease [30]. Furthermore, in unilateral ureteral obstruction-induced fibrotic kidneys, FABP4 inhibition by BMS309403 (BMS) rebalanced abnormal lipid metabolism by restoring impaired FAO in tubular epithelial cells and prevented kidney injury [31]. FABP4 transports free fatty acids to the mitochondria and peroxisomes for FAO, to the endoplasmic reticulum for signal transmission and membrane synthesis, to the nucleus for transcriptional regulation of lipid metabolism-associated genes, and to lipid droplets for storage [32]. FABP4 is mainly expressed in adipocytes and macrophages and plays a significant regulatory role in energy metabolism and inflammation [33].

Clinical studies have shown a negative correlation between serum FABP4 levels and the glomerular filtration rate in DKD patients [34], and FABP4 could be used as a useful prognostic marker for adverse renal outcomes in patients with diabetes [35]. In addition, elevated expression of FABP4 in mesangial and renal tubular epithelial cells may be involved in various kidney diseases, such as acute kidney injury, hyperuricemic nephropathy, and DKD [30]. In renal fibrosis, the expression of FABP4 in renal tubules is upregulated, accompanied by the accumulation of lipid droplets and the downregulation of FAO-associated genes, namely peroxisome proliferator activated receptor gamma (*PPARG*) and carnitine palmitoyltransferase-1 (*CPT1*) [31]. The FABP4 inhibitor BMS restored impaired FAO, reduced lipid accumulation, and prevented kidney injury [31]. Furthermore, a recent study demonstrated that the expression of FABP4 in the retinal tissue of streptozotocin-induced diabetic mice was dramatically elevated, and the inhibition of FABP4 alleviated lipid peroxidation and oxidative stress in diabetic retinopathy by regulating *PPARG*-mediated ferroptosis [36]. These results suggest that FABP4 may be involved in regulating ferroptosis, while its specific mechanism remains to be further studied. Herein, our aim is to clarify the role of FABP4 in ferroptosis linked to DKD.

METHODS

Human renal biopsy

Renal biopsies were collected from patients with established

DKD at the Department of Nephrology in the Seventh Affiliated Hospital of Sun Yat-sen University. The diagnosis was established with standard histological criteria. Participants with other concomitant renal diseases were excluded. For Prussian blue staining and immunofluorescence staining, renal biopsies samples from patients with glomerular minor lesion served as negative controls (NCs). For transmission electron microscopy (TEM) detection, renal biopsies with the diagnosis of early-stage DKD served as NCs. All biopsy issues were obtained with the consent of the patients and were approved by the Ethics Committee of the Seventh Affiliated Hospital of Sun Yat-sen University (KY-2023-024-01).

Chemicals and materials

Dulbecco's modified Eagle's Medium (DMEM)/F12 was obtained from Corning (Corning, NY, USA). DMEM, dimethyl sulfoxide, D-glucose, ferrostatin-1 (Fer-1), and palmitic acid (PA) were acquired from Sigma-Aldrich (St. Louis, MO, USA). Fetal bovine serum (FBS) was purchased from Gibco (Waltham, MA, USA). The FABP4 inhibitor BMS was acquired from ApexBio (Houston, TX, USA). Dojindo (Kumamoto, Japan) provided the cell counting kit-8 (CCK-8). Transfection reagents, small interfering RNA (siRNA)-*FABP4*, si-*CPT1A*, and its NC were acquired from RiboBio (Guangzhou, China). Oil Red O was obtained from Solarbio Science and Technology (Beijing, China). The fatty acid oxidation assay, DCFDA/H2DCFDA–cellular ROS assay kit, and primary antibodies (anti-GPX4, anti-FTH, and anti-FTL) were acquired from Abcam (Cambridge, UK). Anti-FABP4 and anti-CPT1A antibodies were obtained from Proteintech (Wuhan, China). Anti-AMP-activated protein kinase (AMPK) and anti-phospho-AMP-activated protein kinase (p-AMPK) antibodies were acquired from Cell Signaling Technology (Boston, MA, USA). Anti-glyceraldehyde-3-phosphate dehydrogenase (GAPDH) and anti-rabbit/mouse secondary antibodies were acquired from Abclonal (Wuhan, China). Beyotime (Shanghai, China) provided the lipid peroxidation MDA assay kit, terminal deoxynucleotidyl transferase dUTP nick end labeling (TUNEL) apoptosis assay kit, and radioimmunoprecipitation assay (RIPA) lysis buffer. Biological assay systems (Hayward, CA, USA) provided the iron assay kit. Nanjing Jiancheng Bioengineering Institute (Nanjing, China) provided the GSH assay kit and superoxide dismutase (SOD) assay kit. The bicinchoninic acid (BCA) protein assay kit and protease inhibitor were obtained from CWBIO (Jiangsu, China). Polyvinylidene fluoride (PVDF) membranes were obtained from Millipore (Billerica, MA, USA). Bovine serum albumin (BSA) and 2.5% glutaraldehyde were purchased from Servicebio (Wuhan, China).

Cell lines

We purchased human renal proximal tubular epithelial (HK2) cells from Cellcook Biotech Co. Ltd. (Guangzhou, China). We cultured the cells with DMEM/F12 supplemented with 10% FBS and 1% penicillin-streptomycin at 37°C in a humidified incubator with 5% CO_2. In the control group, cells were cultured with DMEM containing 5 mmol/L D-glucose. To establish high glucose (HG)-induced cells, HK2 cells were exposed to 30 mmol/L D-glucose for 48 hours. In the HG+BMS group, cells were cultured in DMEM supplemented with 30 mmol/L D-glucose and 10 μmol/L BMS for 48 hours. In the HG+Fer-1 group, we cultured cells in DMEM medium containing 30 mmol/L D-glucose and 1 μmol/L Fer-1 for 48 hours.

Cell transfection

RiboBio designed and synthesized the siRNAs targeting *FABP4*, *CPT1A*, and the NC. In accordance with the manufacturer's protocol, cells were transfected with NC-siRNA, *FABP4*-siRNA, or *CPT1A*-siRNA at a concentration of 50 nM using transfection reagents from RiboBio. RNA silencing and exogenous expression of FABP4 and CPT1A were optimized with Western blot analysis.

Cell viability assay

First, we exposed HK2 cells to different interventions in 96-well plates with a density of 1×10^4 cells per well, and cultured them for 24, 48, 72 hours, respectively. Then, each well of cells was incubated with 10 μL of the CCK-8 working reagent for 2 hours at 37°C. The absorbance was detected with a microplate reader (Synergy H1M, BioTek, Winooski, VT, USA) at 450 nm. The change in optical density (OD) relative to the baseline was then calculated by subtracting the average OD of the baseline time point (0 hour) from all OD values.

Prussian blue staining

Human kidney tissue paraffin sections were deparaffinized and rehydrated, followed by staining with Prussian blue solution, and images were captured by an upright optical microscope (Nikon Eclipse E100, Nikon, Tokyo, Japan).

Oil Red O staining

Oil Red O staining was used to detect the deposition of neutral lipids in HK2 cells. Cells were washed with phosphate buffered

saline (PBS) twice and fixed in 4% paraformaldehyde at room temperature for 30 minutes. Then, cells were incubated with Oil Red O working solution for 15 minutes in the dark at room temperature. After rinsing with double distilled water (ddH_2O) three times, the cells were then stained with hematoxylin for 1 minute and gently washed with ddH_2O. Finally, light microscopy was used to visualize the cells, and the images were captured at × 400 magnification.

ROS assay

The production of intracellular ROS levels was detected with a DCFDA/H2DCFDA–cellular ROS assay kit. After treatment with HG, with and without BMS or Fer-1, cells were incubated with 10 μmol/L DCFDA for 30 minutes at 37°C in the dark and visualized with fluorescence microscopy.

Iron content detection

The cells were washed with ddH_2O three times and collected with a cell scraper. An ultrasonic crusher was used for homogenization. Supernatants were then collected after centrifuging the cells at 12,000 rpm for 10 minutes at 4°C. We mixed 20 volume units of reagent A, 1 volume unit of ddH_2O, and 1 volume unit of reagent C to prepare the working solution. A total of 50 μL of the diluted standards and 50 μL of the sample were transferred into a 96-well plate, and the working solution (200 μL) was added to each well, followed by incubation for 40 minutes at room temperature in the dark. OD values were then immediately measured at 590 nm.

Measurement of MDA content

MDA levels were measured using the MDA assay kit, following the manufacturer's instructions. Briefly, cells were lysed with RIPA lysis buffer, and the cell lysates were centrifuged at 12,000 rpm for 10 minutes at 4°C to obtain the supernatant. The supernatant of cell lysates (100 μL) was mixed with MDA working solution (200 μL) and incubated at 100°C for 15 minutes. The mixture was centrifuged at 1,000×*g* for 10 minutes after cooling to room temperature, and supernatant (200 μL) was added to a 96-well plate to measure absorbance at 532 nm.

GSH level evaluation

We collected HK2 cells and used an ultrasonic crusher to obtain a homogenate, which was centrifuged at 12,000 rpm for 10 minutes at 4°C, and the supernatant was collected. Samples and standard (100 μL) were respectively added into a 96-well plate, followed by adding 125 μL of the GSH assay mixture into each well and incubating for 5 minutes at room temperature. The absorbance was detected at the wavelength of 405 nm.

SOD assay

The activity of SOD in HK2 cells was examined with the total SOD assay kit (hydroxylamine method). This assay used the xanthine-xanthine oxidase system to produce superoxide ions, which reacted with hydroxylamine to form nitrite, and appeared purple with a chromogenic agent. The absorbance at 550 nm was determined.

FAO enzyme measurements

The analysis of FAO was performed using the fatty acid oxidation assay kit, which detects the expression of FAO enzymes including long chain 3-hydroxyl-coenzyme A (CoA) dehydrogenase (HADHA), acyl-CoA dehydrogenase very long chain (ACADVL), and acyl-CoA dehydrogenase, medium chain specific (ACADM). Cells were washed with PBS, fixed with 4% paraformaldehyde for 15 minutes, permeabilized with 0.1% Triton X-100 in PBS for 15 minutes, and blocked with 5% BSA for 30 minutes. Primary antibodies (HADHA, ACADVL, ACADM) were incubated overnight at 4°C. A fluorescent secondary antibody was incubated for 1 hour at room temperature. 4′,6-Diamidino-2-phenylindole (DAPI) was then used to stain the nuclei for 5 minutes. Finally, an inverted fluorescence microscope was used to capture images.

Western blotting

Cells were washed three times with pre-chilled PBS, homogenized with RIPA lysis buffer containing a protease inhibitor, and centrifuged at 12,000 rpm for 10 minutes at 4°C to collect the supernatant. 5X loading buffer was added to the protein samples and boiled for 6 minutes at 98°C. After electrophoresis in 10% sodium dodecyl sulfate-polyacrylamide gel, the proteins and markers were transferred onto PVDF membranes. Then, a blocking solution of 5% skim milk was applied to membranes for 1 hour at room temperature, followed by incubation with primary antibodies against FABP4, GPX4, FTH, FTL, AMPK, p-AMPK, CPT1A, and GAPDH overnight at 4°C. After washing three times with TBST, the blots were incubated at room temperature for 1 hour with the secondary antibody. Finally, immunoblots were visualized using a chemiluminescence reagent, and AlphaEaseFC software (Alpha Innotech, San Leandro, CA, USA) was used for quantitative densitometry of the protein bands.

Immunofluorescence assay

Immunofluorescence staining was used to detect the expression of FABP4, GPX4, FTH, FTL, and CPT1A in human kidney tissues. The tissue slices were incubated overnight at 4°C with anti-FABP4, anti-GPX4, anti-FTH, anti-FTL, and anti-CPT1A antibodies, respectively. Then, the slices were incubated at room temperature for 50 minutes with the secondary antibody, which was labeled with fluorescein. DAPI was then used to stain nuclei for 10 minutes. Finally, an ortho-fluorescence microscope (Nikon Eclipse C1) was used to capture images.

Transmission electron microscopy

We fixed HK2 cells with 2.5% glutaraldehyde for 2 to 4 hours at 4°C and wrapped them with 1% agarose. Next, cells were fixed with 1% aqueous osmium tetroxide for 2 hours, dehydrated in gradual ethanol (50% to 100%) and 100% acetone, followed by embedding with embedding agents in an oven at 37°C overnight and curing at 60°C for 48 hours. We cut ultrathin sections of 60 to 80 nm and stained them with 2% uranyl acetate-saturated alcohol solution and 2.6% lead citrate for 15 minutes. The sections were dried overnight at room temperature. Eventually, we used TEM (HT7700-SS, Hitachi, Tokyo, Japan) to observe and capture images.

Statistical analysis

Prism version 8.0 (GraphPad, La Jolla, CA, USA) was used to perform statistical analyses. The results were presented as mean±standard deviation. One-way analysis of variance followed by the Tukey multiple-comparison test was applied for multiple comparisons. The Student's *t* test was used for comparisons between two groups. *P* values <0.05 were considered to indicate statistical significance.

RESULTS

DKD patient biopsies

In DKD patients, the renal tubules showed iron accumulation, as detected by Prussian blue staining (Fig. 1A), whereas TEM showed reduced mitochondrial volume and loss of cristae (Fig. 1B). These morphological changes are consistent with ferroptosis. In addition, the expression of ferroptosis-related proteins, including GPX4, FTH, and FTL, were reduced (Fig. 2A). These alterations in ferroptosis-related indicators suggest that ferroptosis is involved in diabetic kidney injury. In kidney biopsy tissues, the expression of FABP4 was upregulated in both renal tubules and glomerulus, compared to non-DKD patients (Fig. 2B), whereas the expression of CPT1A was reduced (Fig. 2C).

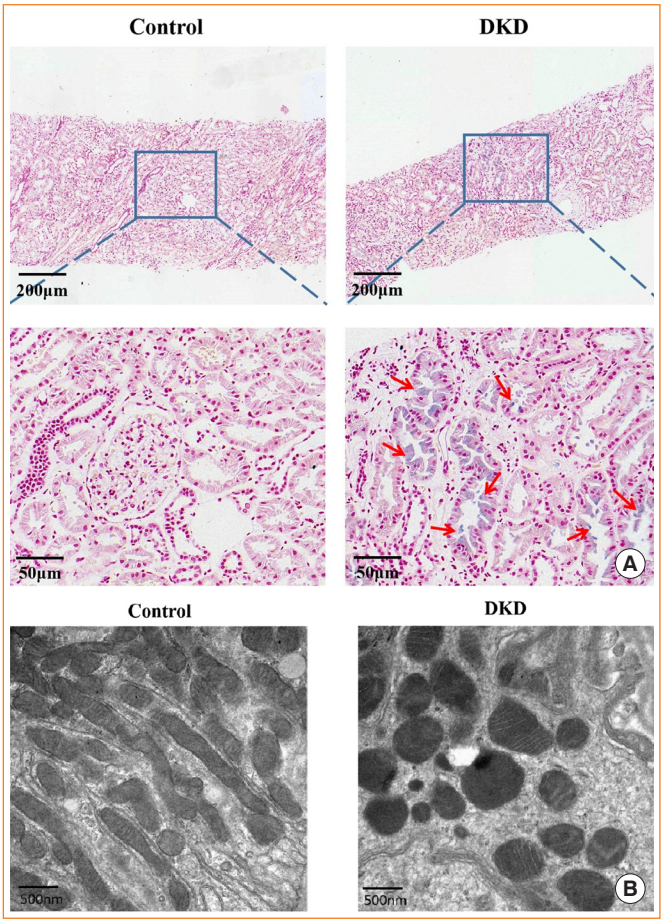

Fig. 1. Changes related to ferroptosis in biopsies of diabetic kidney disease (DKD) patients. (A) Prussian blue staining of kidney biopsy tissue. The red arrows indicate iron deposition. Control refers to patients with glomerular minor lesion. (B) Transmission electron microscopy images of mitochondria in renal proximal tubular epithelial cells. Control refers to patients with early-stage DKD.

Involvement of ferroptosis in HG-induced HK2 cells

To explore whether ferroptosis is involved in HG-induced renal tubule injury, we treated HK2 cells with the ferroptosis inhibitor Fer-1 in medium containing HG for 48 hours. HG-HK2 cells were less viable than the control group, and exposure to Fer-1 increased the cell viability (Fig. 3A). In the HG group, the levels of Fe^{2+} and the lipid peroxidation product MDA were increased, whereas SOD and GSH levels and the expression of GPX4, FTH, FTL, and p-AMPK were decreased (Fig. 3B-H). HK2 cells were stained with DCFDA/H2DCFDA to detect ROS generation. Compared to the control group, intracellular ROS levels were increased in HG-HK2 cells, but decreased after Fer-

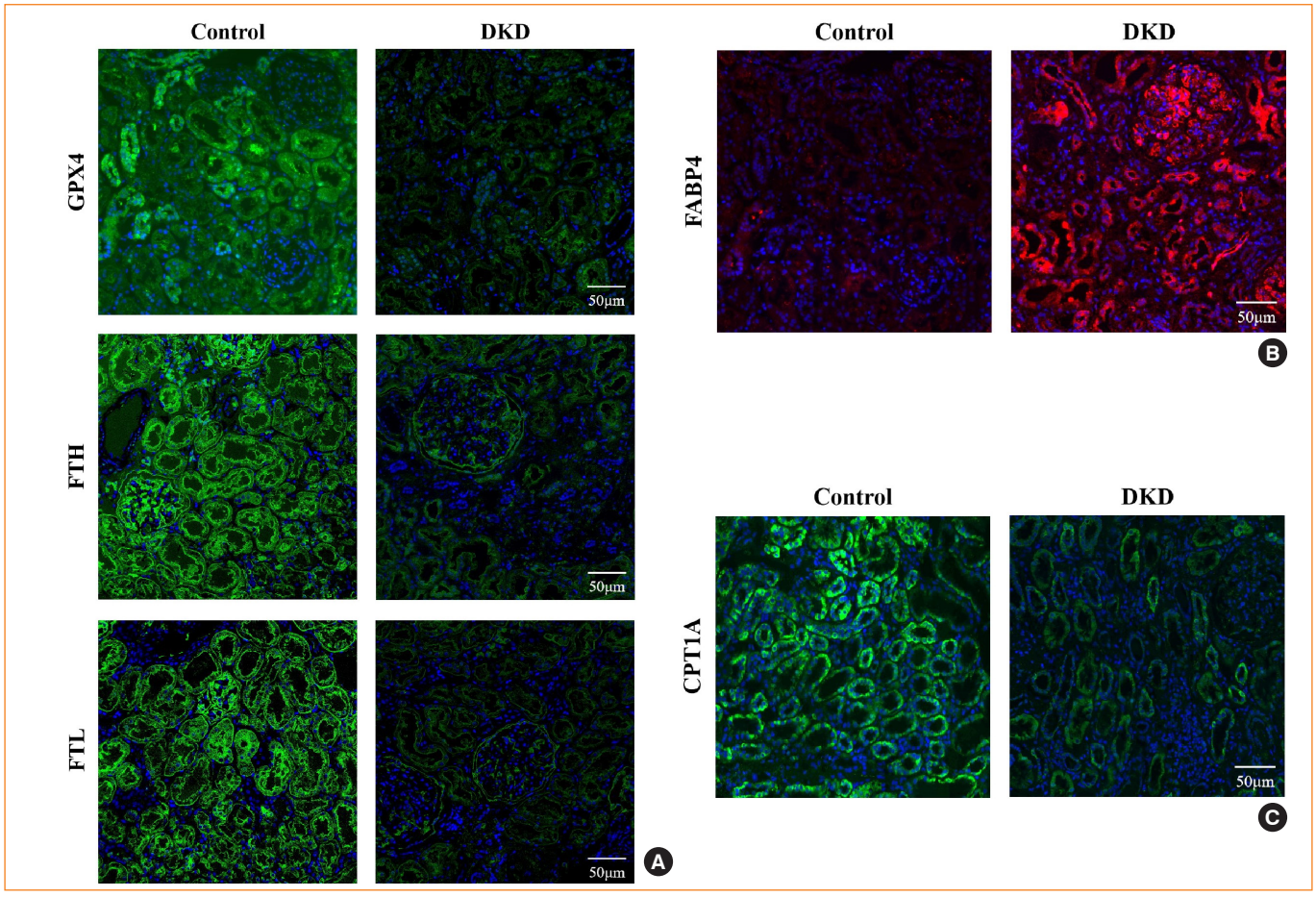

Fig. 2. Expression of fatty acid binding protein 4 (FABP4) and ferroptosis-associated proteins in diabetic kidney disease (DKD) patients. Representative immunofluorescence images of kidney tissue sections in negative controls and DKD patients for (A) glutathione peroxidase 4 (GPX4), ferritin heavy chain (FTH), and ferritin light chain (FTL), (B) FABP4, and (C) carnitine palmitoyltransferase-1A (CPT1A). 4′,6-Diamidino-2-phenylindole (DAPI) indicates nuclear staining.

1 treatment (Fig. 3I). HG-treated cells showed mitochondrial cristae reduction or even disappearance, and mitochondrial outer membrane rupture (Fig. 3J). In summary, ferroptosis inhibitor Fer-1 reverted the changes induced by HG, suggesting that HG could induce ferroptosis in HK2 cells.

Involvement of FABP4 in HG-induced ferroptosis in HK2 cells

To explore whether FABP4 is involved in HG-induced ferroptosis, HK2 cells were treated with the FABP4 inhibitor BMS. FABP4 expression was clearly upregulated in HG-HK2 cells and decreased after BMS treatment (Fig. 4A). FABP4 inhibition reverted the changes induced by HG: increased cell viability (Fig. 4B), reduced cell death (Fig. 4C), reduced abnormally high intracellular levels of Fe^{2+} (Fig. 4D), MDA (Fig. 4E), and ROS (Fig. 4K), increased abnormally low levels of SOD (Fig. 4F), increased FTH and FTL expression (Fig. 4I), and attenuated morphological changes in mitochondria (Fig. 4L). However, there was no statistically significant difference in changes of GSH and GPX4 after BMS treatment (Fig. 4G, H). Thus, FABP4 inhibition reversed the characteristic effects of ferroptosis in HG-HK2 cells. In addition, we also measured p-AMPK levels in HK2 cells under HG conditions. The results indicated that the expression of p-AMPK decreased in HG-HK2 cells. However, BMS could not reverse this change (Fig. 4J).

To further clarify the effect of FABP4 on ferroptosis, HG-HK2 cells were transfected with *FABP4*-siRNA. Western blots showed that FABP4 was downregulated after transfection (Fig. 5A). Similarly, *FABP4* silence significantly increased the cell viability under HG conditions (Fig. 5B). Besides, lower levels of Fe^{2+}, ROS and MDA, and increased levels of SOD were also detected in the HG+FABP4-siRNA group compared with the HG+NC-

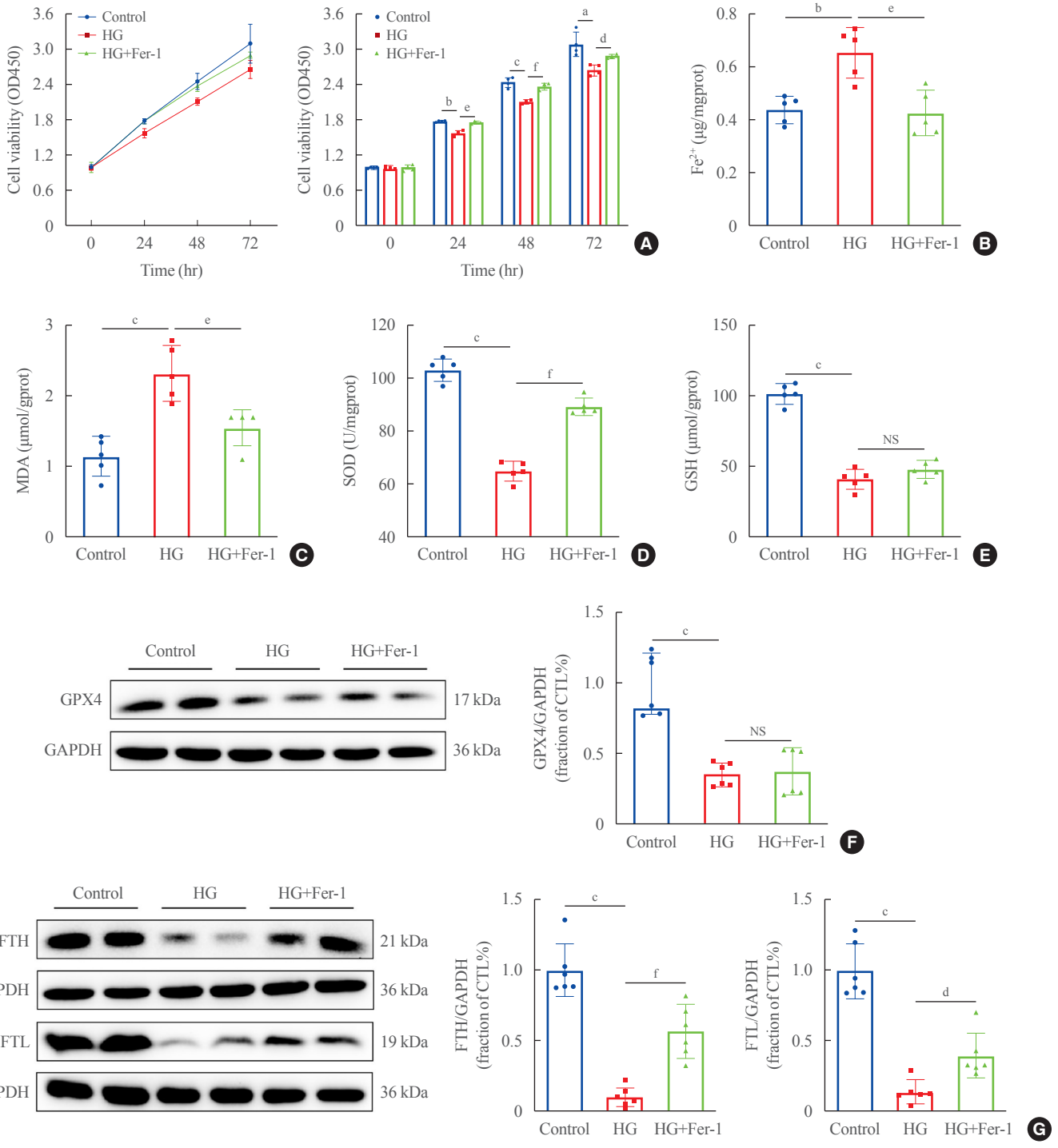

Fig. 3. Ferroptosis-related changes induced by high glucose in human renal proximal tubular epithelial (HG-HK2) cells. (A) Viability of HK2 cells detected by cell counting kit-8 (CCK-8) in the three groups indicated. Levels of (B) ferrous iron (Fe^{2+}), (C) malondialdehyde (MDA), (D) superoxide dismutase (SOD), and (E) glutathione (GSH) in the control, HG, and HG+ferrostatin-1 (Fer-1) groups. Protein expression of (F) glutathione peroxidase 4 (GPX4), (G) ferritin heavy chain (FTH), ferritin light chain (FTL), and (H) phospho-AMP-activated protein kinase (p-AMPK) in the three groups. (I) Intracellular reactive oxygen species (ROS) production stained with DCFDA/H2DCFDA fluorescent probes. (J) Mitochondrial morphology detected by transmission electron microscopy. The red arrows indicate the damaged mitochondria (mitochondria cristae vanish and membrane rupture). NS, no statistical significance; GAPDH, glyceraldehyde-3-phosphate dehydrogenase; CTL, control. $^{a}P<0.05$, $^{b}P<0.01$, $^{c}P<0.001$ when compared with the control group; $^{d}P<0.05$, $^{e}P<0.01$, $^{f}P<0.001$ when compared with the HG group. (*Continued to the next page*)

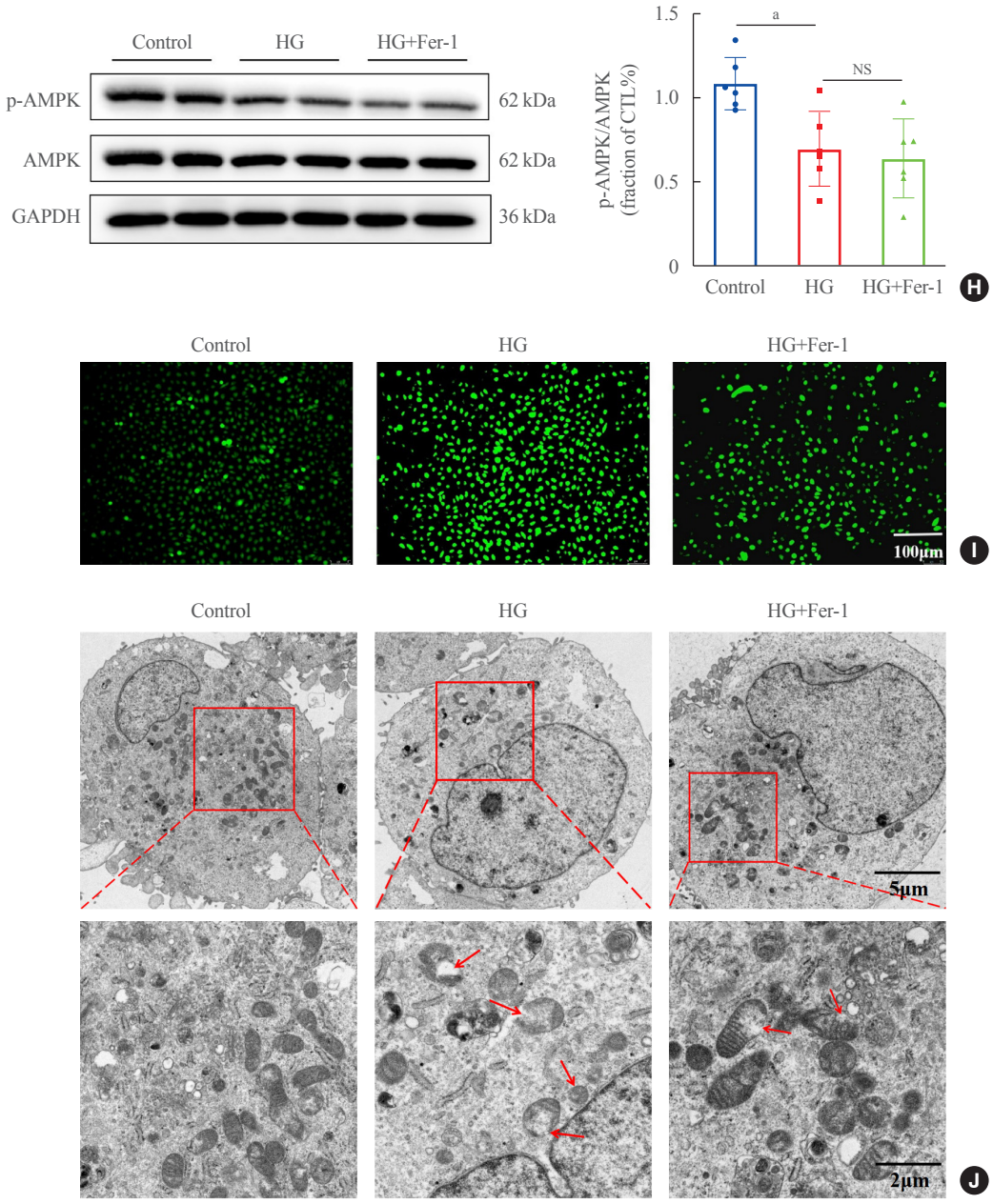

Fig. 3. Continued.

siRNA group (Fig. 5C-G). The above results suggested that FABP4 was involved in HG- induced ferroptosis in HK2 cells and inhibition of FABP4 could protect cells from ferroptosis.

Mediation of HG-induced ferroptosis by FABP4, most likely through inhibiting FAO

Since the inhibition of FAO increases the sensitivity to ferroptosis, we explored whether FABP4 regulated HG-induced ferroptosis by inhibiting FAO. In HG-HK2 cells, expression of CPT1A, the rate-limiting enzyme for FAO, was reduced, and recovered after FABP4 inhibition by BMS (Fig. 6A). As showed by immunofluorescence assays, compared with the control group, the expression levels of key enzymes involved in FAO pathway (HADHA, ACADVL, and ACADM) decreased in HG-HK2 cells, which could be reversed by BMS (Fig. 6B). In addition, the abnormal accumulation of lipid droplets is considered to be a marker for dysregulation of fatty acid metabolism. We also detected the intracellular lipid deposition by Oil Red O staining, which demonstrated that lipid deposition was elevated in HG-HK2 cells. However, this was reduced after FABP4 inhibition by

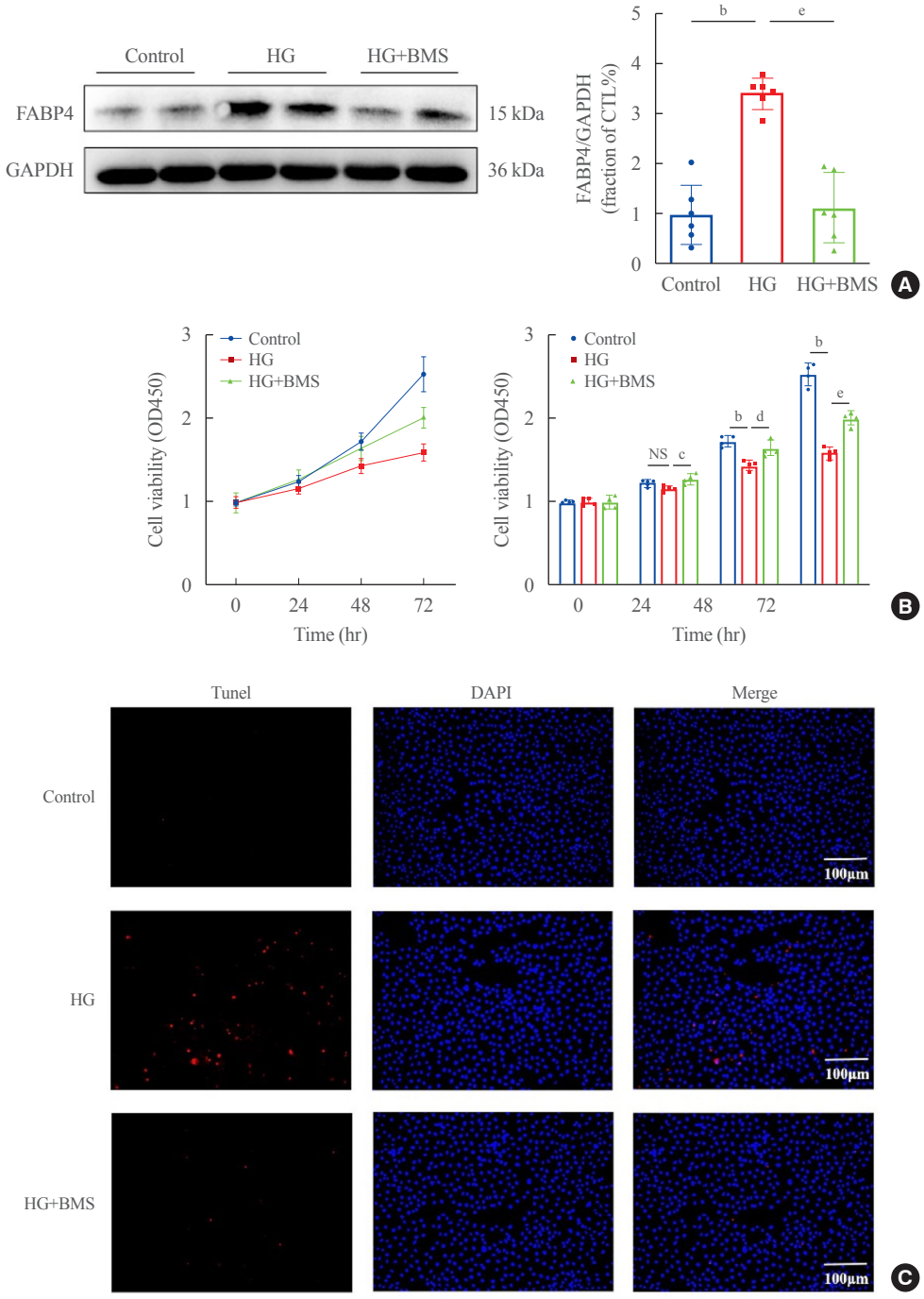

Fig. 4. Inhibition of fatty acid binding protein 4 (FABP4) by BMS309403 (BMS) attenuated ferroptosis induced by high glucose in human renal proximal tubular epithelial (HG-HK2) cells. (A) Expression of FABP4 in the three groups indicated. (B) Viability of cells in the three groups indicated. (C) Representative images of cell death measured by terminal deoxynucleotidyl transferase dUTP nick end labeling (Tunel) staining (positive=red), where the nucleus is labeled with 4′,6-diamidino-2-phenylindole (DAPI; blue). Concentrations of (D) ferrous iron (Fe^{2+}), (E) malondialdehyde (MDA), (F) superoxide dismutase (SOD), (G) glutathione (GSH), (H) expression of glutathione peroxidase 4 (GPX4), (I) ferritin heavy chain (FTH), ferritin light chain (FTL), and (J) phospho-AMP-activated protein kinase (p-AMPK) in each group. (K) Content of reactive oxygen species (ROS) stained with DCFDA/H2DCFDA fluorescent probes. (L) Mitochondrial morphology detected by transmission electron microscopy. The red arrows indicate the damaged mitochondria (mitochondria cristae vanish and membrane rupture). NS, no statistical significance; GAPDH, glyceraldehyde-3-phosphate dehydrogenase; CTL, control. $^{a}P<0.01$, $^{b}P<0.001$ when compared with the control group; $^{c}P<0.05$, $^{d}P<0.01$, $^{e}P<0.001$ when compared with the HG group. (*Continued to the next page*)

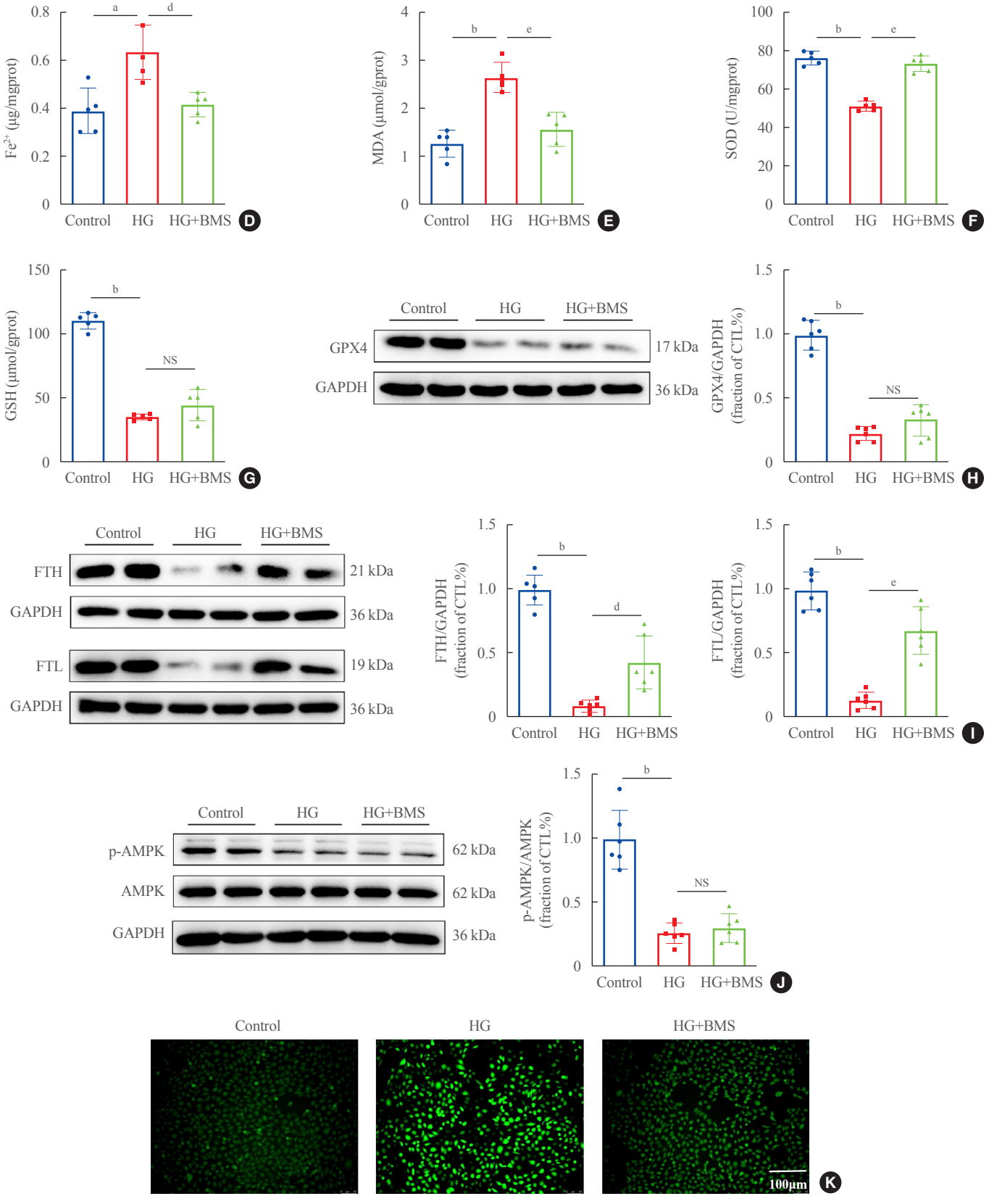

Fig. 4. Continued.

(*Continued to the next page*)

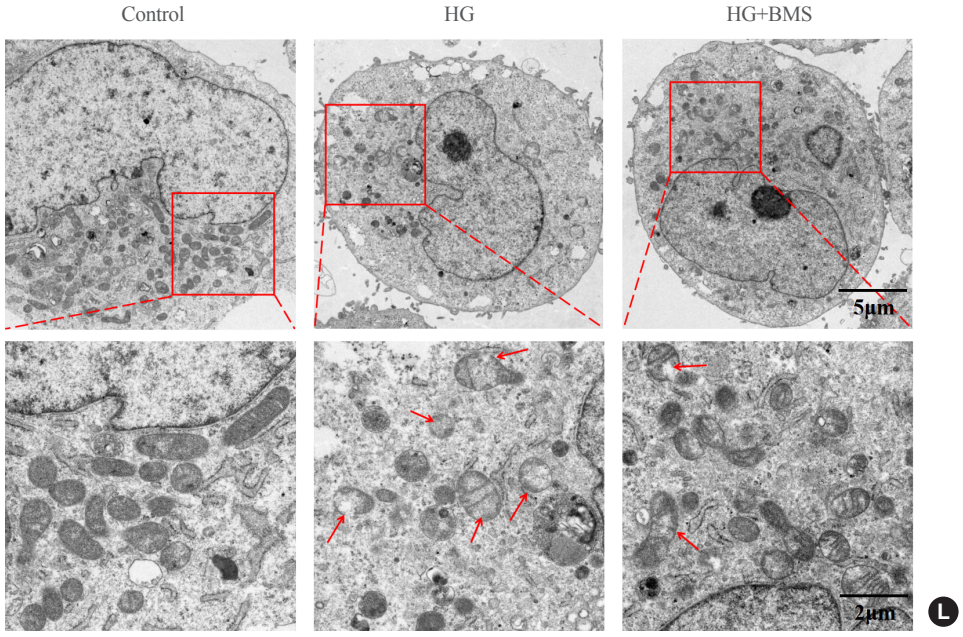

Fig. 4. Continued.

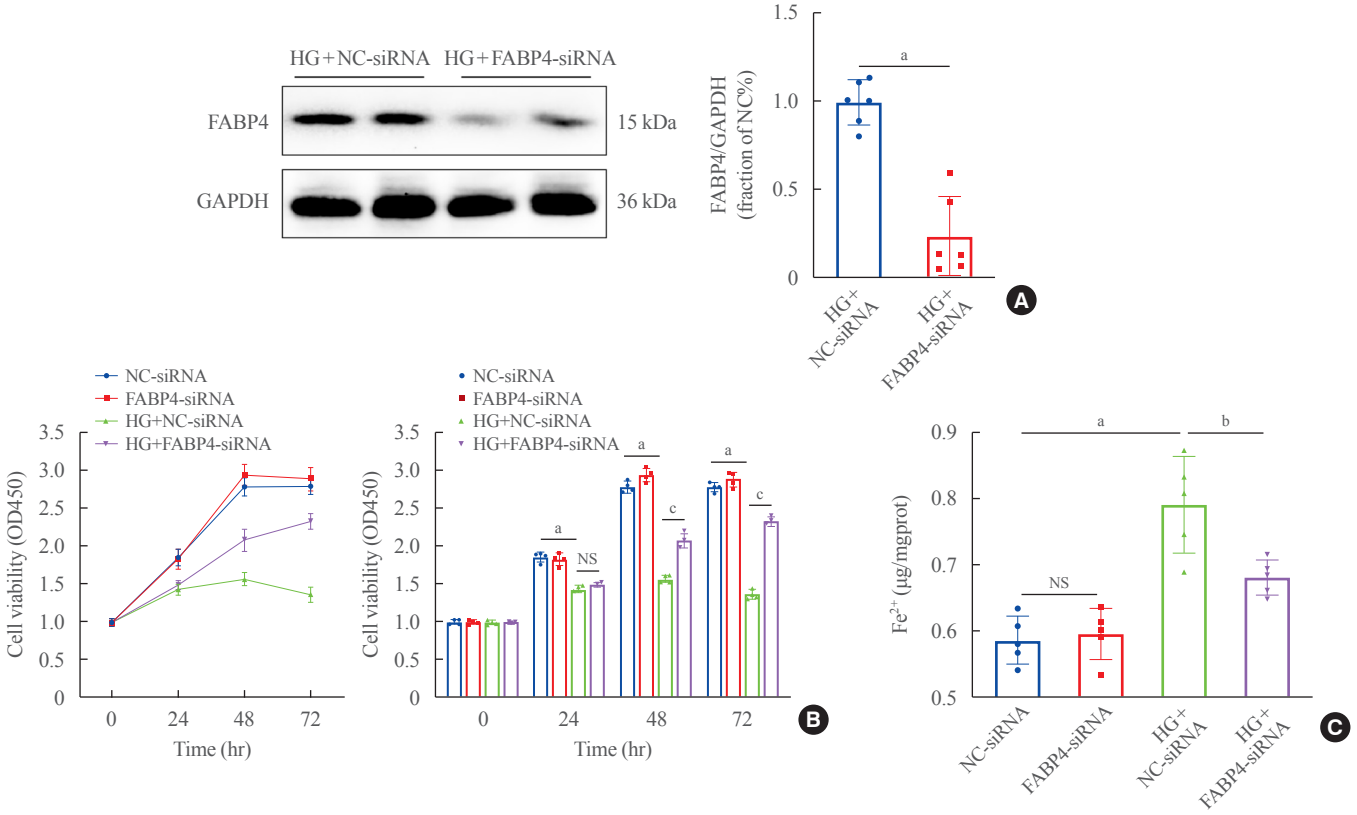

Fig. 5. Silencing fatty acid binding protein 4 (*FABP4*) inhibited ferroptosis induced by high glucose in human renal proximal tubular epithelial (HG-HK2) cells. (A) Expression of FABP4 after transfection with *FABP4*-small interfering RNA (siRNA). (B) Effect of silencing *FABP4* on cell viability. Concentrations of (C) ferrous iron (Fe^{2+}), (D) malondialdehyde (MDA), (E) superoxide dismutase (SOD), and (F) glutathione (GSH). (G) Reactive oxygen species (ROS) stained with DCFDA/H2DCFDA fluorescent probes. GAPDH, glyceraldehyde-3-phosphate dehydrogenase; NS, no statistical significance. [a]$P<0.001$ compared with the negative control (NC)-siRNA group; [b]$P<0.01$, [c]$P<0.001$ compared with the HG+NC-siRNA group.

(*Continued to the next page*)

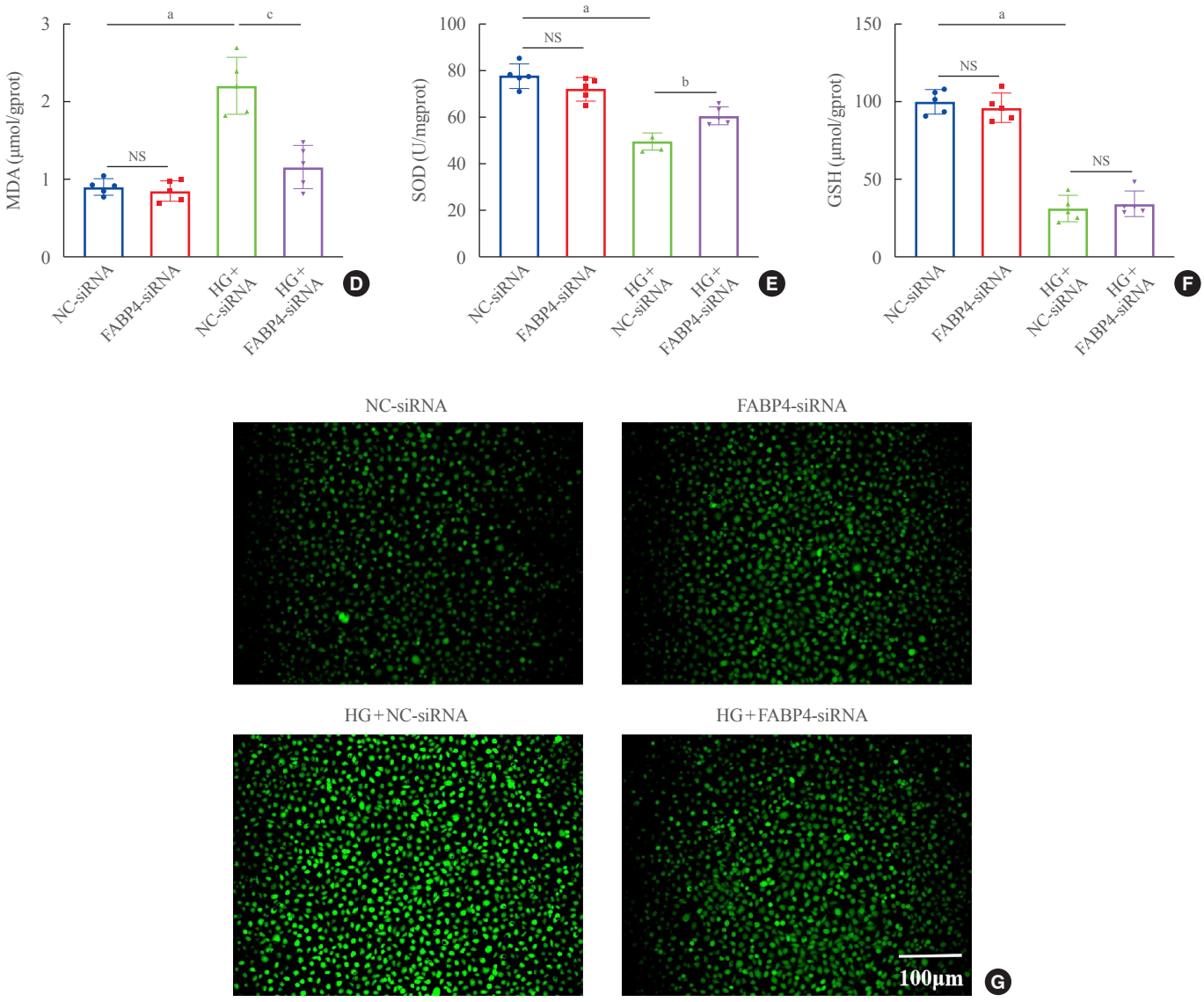

Fig. 5. Continued.

BMS (Fig. 6C). These results collectively indicated that the inhibition of FABP4 could restore impaired FAO induced by HG.

To further characterize the involvement of lipid deposition induced by FABP4 and impaired FAO in HG-induced ferroptosis, we cultured HK2 cells with PA, and treated them with or without BMS. When HK2 cells were exposed to PA, lipid accumulation, and ferroptosis-associated mitochondrial damage were observed, and these effects were also reduced after FABP4 inhibition by BMS (Fig. 6C, D). Furthermore, in order to identify whether the inhibition of FAO could promote ferroptosis in HK2 cells, we also transfected HK2 cells with *CPT1A*-siRNA and detected ferroptosis-related indicators. Western blot showed that CPT1A was downregulated after transfection (Fig. 7A). After being transfected with *CPT1A*-siRNA, cell viability significantly decreased (Fig. 7B), the levels of ROS, Fe^{2+}, and MDA increased, whereas SOD and GSH decreased (Fig. 7C-G). Similarly, these changes could be reversed by Fer-1, indicating that inhibition of CPT1A could induce ferroptosis in HK2 cells. Overall, these results suggest a link between impaired FAO induced by FABP4 and ferroptosis in HG-HK2 cells. FABP4 increased the sensitivity of HK2 cells to ferroptosis by inhibiting FAO and aggravating lipid accumulation.

DISCUSSION

In the present study, we showed that the expression of FABP4

was elevated in DKD patients, whereas that of CPT1A, GPX4, FTH, and FTL was reduced. This was accompanied by iron deposition in renal tubules and the disappearance of mitochondrial cristae, characteristic of ferroptosis. Using HG-HK2 cells, we also showed that ferroptosis was involved in HG-induced tubular injury. In HG-HK2 cells, FABP4 was upregulated, whereas FABP4 inhibition abrogated lipid accumulation and peroxidation by restoring FAO. The inhibition of FABP4 increased the resistance to ferroptosis in HK2 cells, suggesting that FABP4 played a regulatory role in the HG-induced ferroptosis of renal tubular cells, and FABP4 may serve as a new therapeutic target in DKD.

Our study showed that the pharmacological and genetic inhibition of FABP4 improved cell viability, prevented ROS and

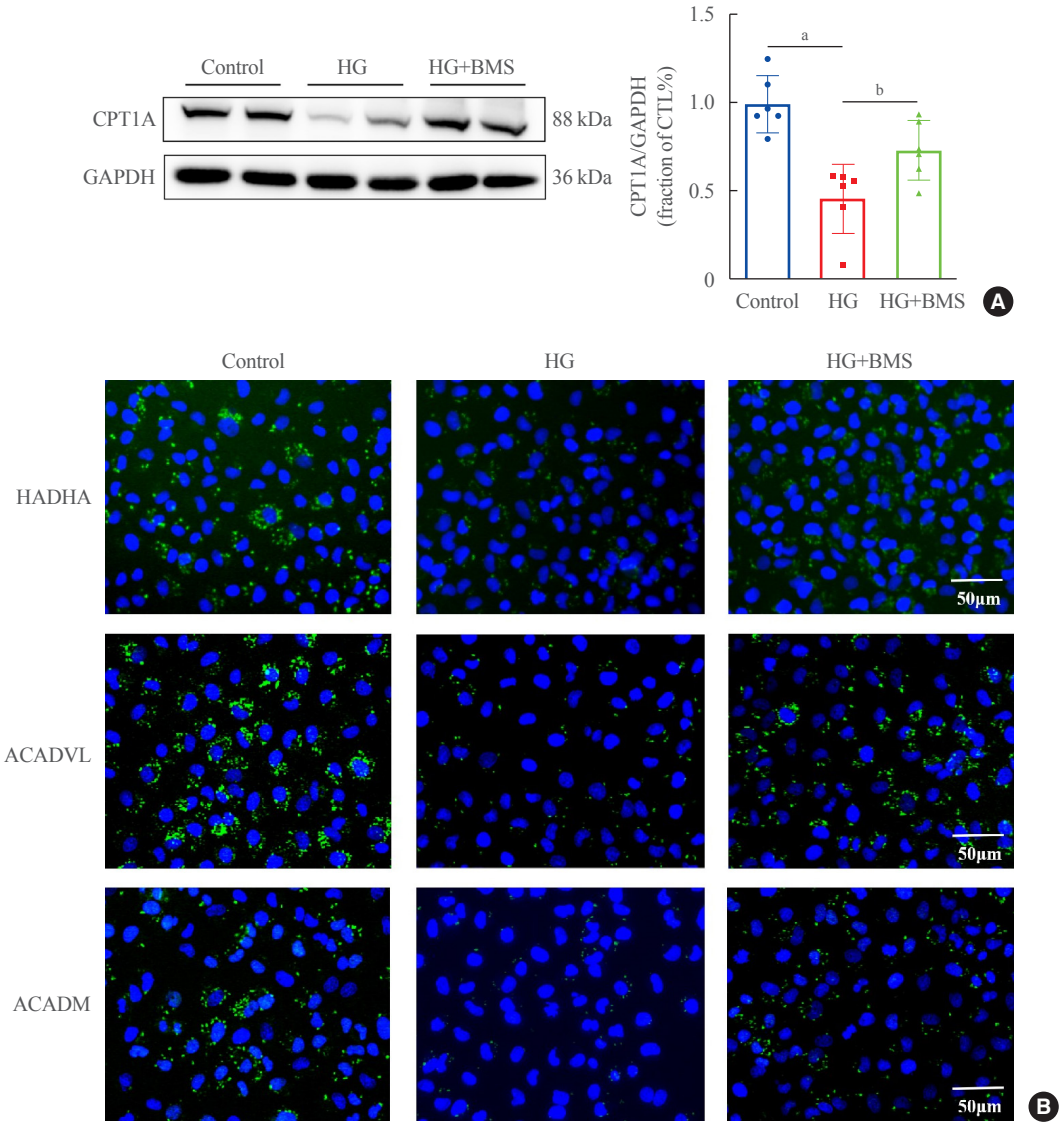

Fig. 6. Inhibition of fatty acid binding protein 4 (FABP4) restores impaired fatty acid β-oxidation in human renal proximal tubular epithelial (HK2) cells. (A) Protein expression of carnitine palmitoyltransferase-1A (CPT1A) in HK2 cells for the three groups indicated. (B) Representative immunofluorescence images of HK2 cells for long chain 3-hydroxyl-coenzyme A (CoA) dehydrogenase (HADHA), acyl-CoA dehydrogenase very long chain (ACADVL), and acyl-CoA dehydrogenase, medium chain specific (ACADM). (C) Lipid accumulation after high glucose (HG) and palmitic acid (PA) stimulation, with and without BMS309403 (BMS), as detected by Oil Red O staining. The red arrows indicate lipid droplets. (D) Mitochondrial morphology in HG, HG+PA, and HG+PA+BMS groups. The red arrows indicate the damaged mitochondria (mitochondria cristae vanish and membrane rupture). GAPDH, glyceraldehyde-3-phosphate dehydrogenase; CTL, control. [a]$P<0.001$ compared with the control group; [b]$P<0.05$ compared with the HG group. (*Continued to the next page*)

MDA production, and reduced intracellular iron levels in HG-HK2 cells, indicating that inhibiting FABP4 can suppress lipid peroxidation and ferroptosis. FABP4 can mediate ferroptosis and exacerbate the progression of DKD. Indeed, previous reports have shown that *FABP4* knockout inhibits inflammation and apoptosis in kidney tubules and improves renal dysfunction in rhabdomyolysis-induced AKI [37]. FABP4 was also found to be involved in ferroptosis in cancer and diabetic retinopathy by regulating lipid metabolism [36,38]. Ferroptosis is regulated by multiple metabolic pathways [39-41], and one main characteris-

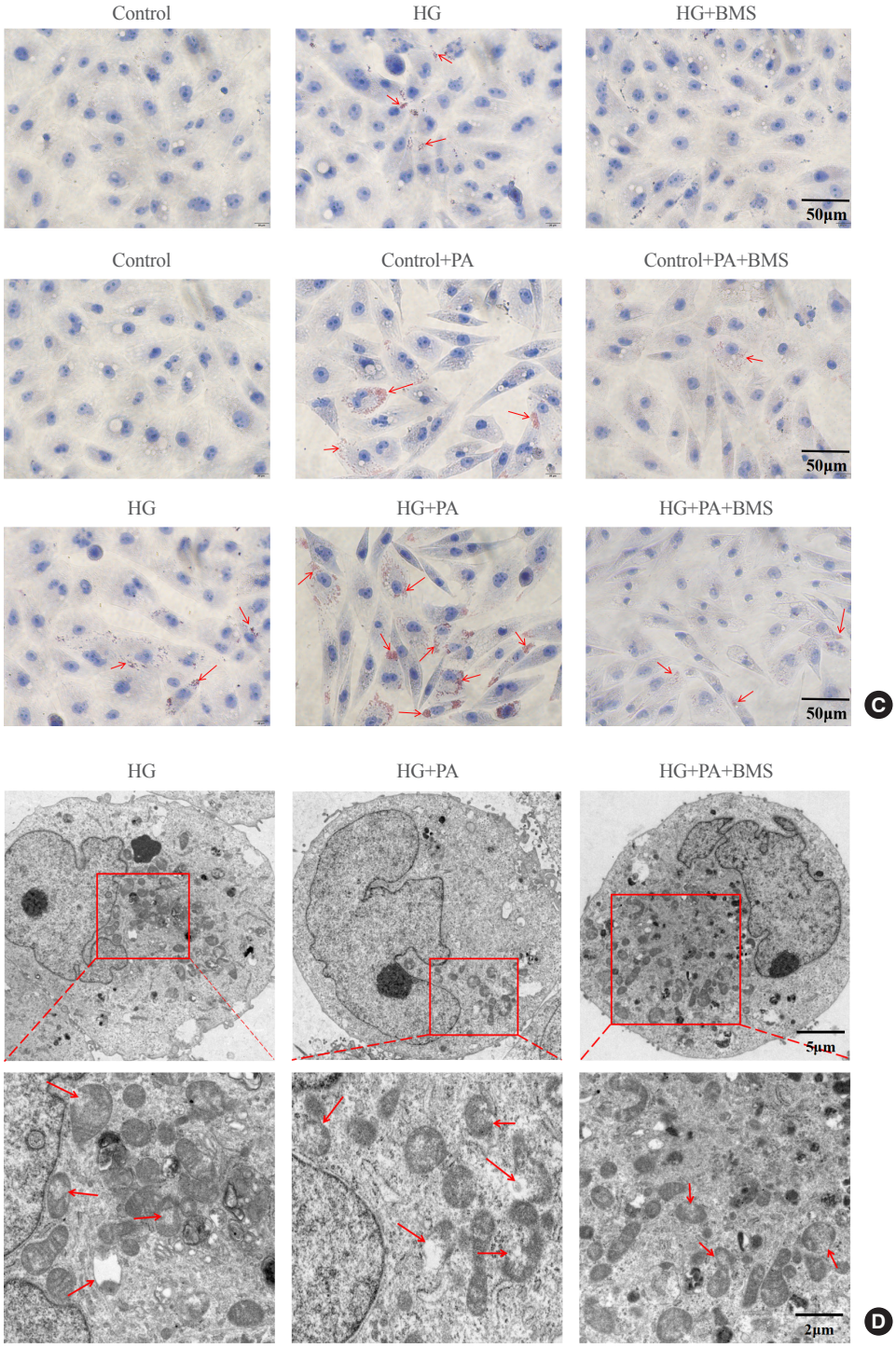

Fig. 6. Continued.

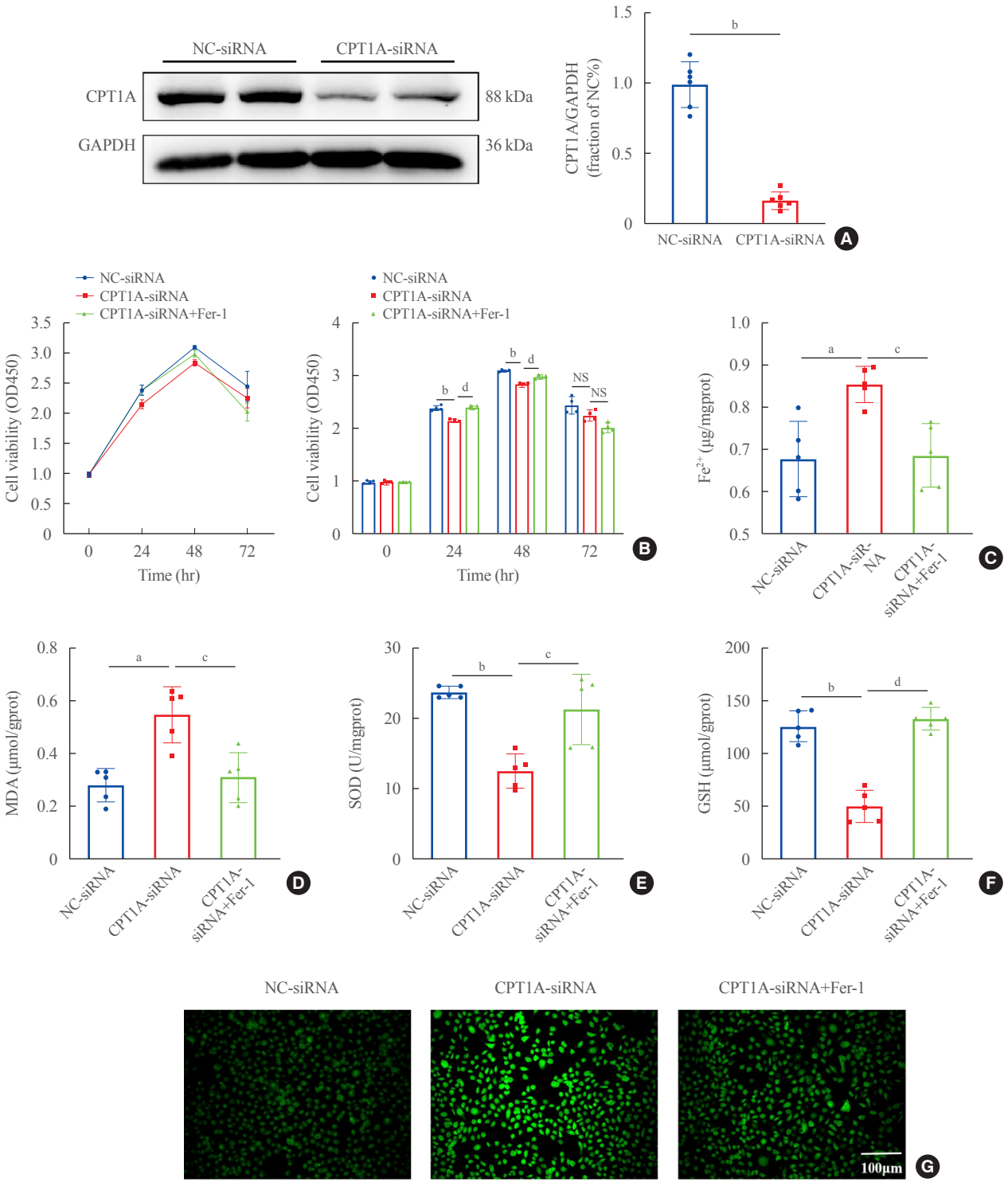

Fig. 7. Silencing carnitine palmitoyltransferase-1A (*CPT1A*) induced ferroptosis in human renal proximal tubular epithelial (HK2) cells. (A) Expression of CPT1A after transfection with *CPT1A*-small interfering RNA (siRNA). (B) Effect of silencing *CPT1A* on cell viability. Concentrations of (C) ferrous iron (Fe^{2+}), (D) malondialdehyde (MDA), (E) superoxide dismutase (SOD), and (F) glutathione (GSH). (G) Reactive oxygen species (ROS) content stained with DCFDA/H2DCFDA fluorescent probes. GAPDH, glyceraldehyde-3-phosphate dehydrogenase; Fer-1, ferrostatin-1; NS, no statistical significance. $^{a}P<0.01$, $^{b}P<0.001$ compared with the negative control (NC)-siRNA group; $^{c}P<0.01$, $^{d}P<0.001$ compared with the CPT1A-siRNA group.

tic is lipid peroxidation, which could be driven by abnormal lipid metabolism. It is known that lipid metabolism modulates ferroptosis sensitivity or tolerance in different disease models [42]. Polyunsaturated fatty acids (PUFAs) are most susceptible to lipid peroxidation, and the peroxidation of PUFA-containing membrane phospholipids (PUFA-PLs) is the key trigger of ferroptosis [43]. PUFAs are converted to PUFA-CoA and incorporated into phospholipids to form PUFA-PLs, which are peroxidized by iron-dependent ROS, triggering ferroptosis [42]. The inhibition of FAO increases sensitivity to ferroptosis, probably because it leads to the accumulation of free fatty acids, such as PUFAs, which serve as a substrate for peroxidation [23].

In contrast to PUFAs, monounsaturated fatty acids (MUFAs) can protect cells against ferroptosis by inhibiting the accumulation of lipid ROS in cell membranes and reducing PUFA incorporation into phospholipids [44]. Previous studies have shown that under glucose deprivation conditions, the depletion of adenosine triphosphate (ATP) activates the AMPK pathway, which suppresses the synthesis of MUFAs by phosphorylating and inhibiting acetyl-CoA carboxylase, and thus prevents ferroptosis [45]. Studies have also indicated that AMPK dysregulation plays an essential role in the progression of DKD [46]. Physiologically, when AMPK is activated, it promotes energy-producing catabolic pathways and inhibits anabolic pathways, maintaining the energy metabolism balance [47]. However, in diabetic conditions, the phosphorylation of AMPK is suppressed, which results in abnormal glucose and lipid metabolism [46]. Considering that AMPK activation is responsible for ferroptosis

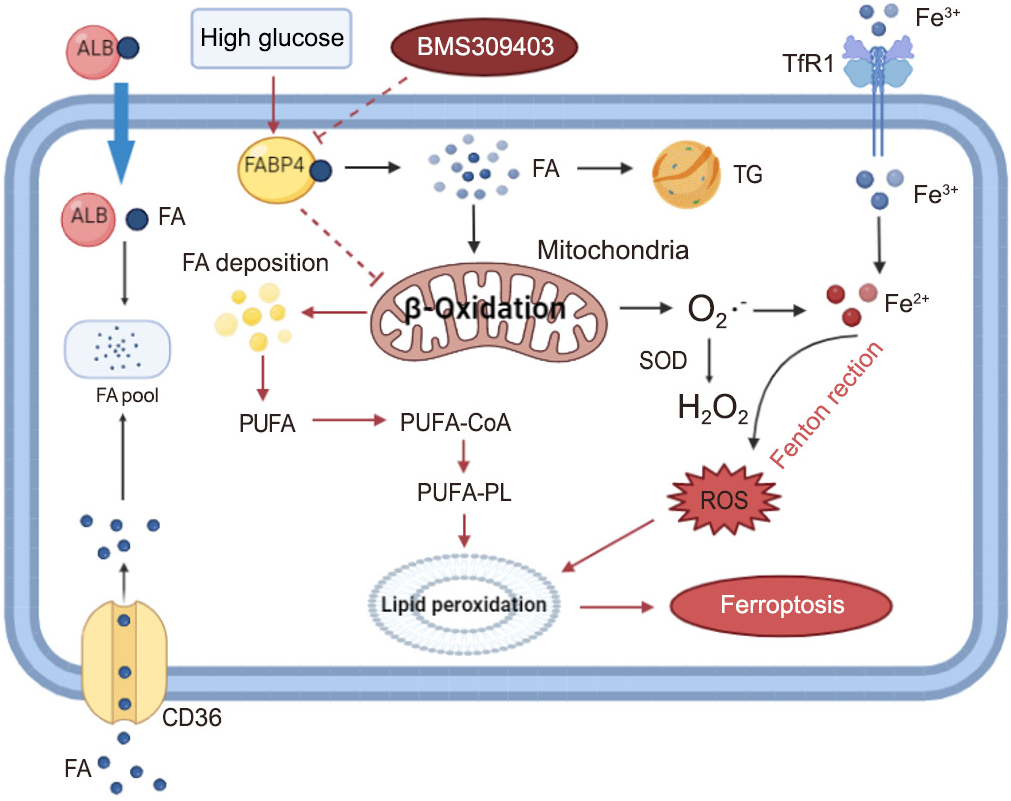

Fig. 8. Potential mechanism of fatty acid binding protein 4 (FABP4) involvement in ferroptosis-mediated renal tubule injury induced by high glucose. Physiologically, fatty acids are taken up from the basolateral membrane by proximal renal tubular epithelial cells through the cluster of differentiation 36 (CD36) receptor; and from the apical membrane through endocytosis in albumin-bound form. In the cell, they are converted to fatty acyl-coenzyme A (CoA) and are transported to mitochondria for fatty acid β-oxidation (FAO). In diabetes (red arrow), high glucose upregulates FABP4 expression in renal tubular cells, which inhibits FAO through downregulating carnitine palmitoyltransferase-1 (CPT1) and leads to lipid accumulation, providing more substrate for lipid peroxidation. Polyunsaturated fatty acids (PUFAs) are converted to PUFA-CoA and are incorporated into PUFA-phospholipids, which react with iron-dependent reactive oxygen species (ROS) and induce lipid peroxidation and ferroptosis. ALB, albumin; FA, fatty acid; Fe^{3+}, ferric iron; TfR1, transferrin receptor 1; TG, triglycerides; Fe^{2+}, ferrous iron; O_2^-, superoxide anion; SOD, superoxide dismutase; H_2O_2, hydrogen peroxide; PL, phospholipid.

suppression, we also measured the expression level of p-AMPK in HK2 cells under HG conditions. Our results indicated that p-AMPK expression was decreased in HG-HK2 cells, indicating that AMPK phosphorylation was inhibited in HG conditions. However, BMS could not reverse this change, indicating that BMS inhibited ferroptosis via an AMPK-independent pathway.

The normal physiological activity of kidney tubule cells requires FAO to generate ATP [48]. Fatty acids are primarily taken up by renal tubules from the basolateral membrane through cluster of differentiation 36 (CD36) receptors and fatty acid transporting protein (Fig. 8), and also through the apical membrane by endocytosis in albumin-bound form [49]. Free fatty acids that enter into the cell are converted to fatty acyl-CoA and transported to mitochondria via CPT1, entering the FAO pathway [50]. Impaired FAO is a primary mechanism of tubular damage and fibrosis in renal disease, and renal tubule-specific overexpression of *CPT1* was shown to reduce kidney injury and fibrosis [51]. Herein, we found that HG-HK2 cells exhibited downregulated CPT1A expression and abnormal lipid accumulation, consistent with FAO inhibition. Conversely, FABP4 inhibition restored FAO and attenuated abnormal lipid deposition. We confirmed that the inhibition of FAO by transfecting HK2 cells with *CPT1A*-siRNA could promote ferroptosis. In addition, by exposing HK2 cells to PA, we also found that lipid deposition could induce ferroptosis. Thus, the inhibition of FABP4 suppresses lipid peroxidation and ferroptosis, partly by restoring FAO and attenuating abnormal lipid accumulation.

In DKD patients, previous studies have shown heavy lipid deposition in podocytes, tubular epithelial cells and mesangial cells, together with the dysregulation of lipid metabolism genes [26]. The dysregulation of the formation, oxidation, and uptake of lipids leads to ectopic lipid accumulation in the kidneys and may contribute to DKD progression [52-54]. Renal lipid deposition may cause renal injury by activating the inflammatory response, ROS production, mitochondrial dysfunction, endoplasmic reticulum stress, and apoptosis [24,49]. Herein, we showed that FABP4 triggered ferroptosis by inhibiting FAO, revealing an association between abnormal lipid metabolism and ferroptosis in DKD. Since ferroptosis is triggered by the peroxidation of PUFAs in cell membrane phospholipids [42,43], the accumulation of PUFAs due to impaired FAO could increase lipid peroxidation and thereby induce ferroptosis [22]. Nevertheless, the specific mechanism through which FABP4 mediates ferroptosis by inhibiting FAO remains to be further studied in the future.

In conclusion, our study indicated that FABP4 mediated ferroptosis in HG-HK2 cells by inhibiting FAO. This suggests that targeting FABP4 and ferroptosis in DKD may be a novel therapeutic strategy.

CONFLICTS OF INTEREST

No potential conflict of interest relevant to this article was reported.

ACKNOWLEDGMENTS

This work was supported by the Sanming Project of Medicine in Shenzhen (SZSM201911013), the National Nature Science Foundation of China (82170690), The Shenzhen Science and Technology Innovation Committee of Guangdong Province of China (JCYJ20180307150634856, JCYJ20210324123200003).

AUTHOR CONTRIBUTIONS

Conception or design: J.C., K.W., Y.L., M.H., L.C., H.G., J.L., M.Z., X.W., Z.Z. Acquisition, analysis, or interpretation of data: J.C., K.W., M.H., L.C., H.G., J.L., M.Z., X.W. Drafting the work or revising: J.C., K.W., Y.L., Z.Z. Final approval of the manuscript: J.C., K.W., Y.L., M.H., L.C., H.G., J.L., M.Z., X. W., Z.Z.

ORCID

Jiasi Chen *https://orcid.org/0000-0002-3759-8574*
Keping Wu *https://orcid.org/0000-0002-1440-8766*
Yan Lei *https://orcid.org/0000-0001-7075-0438*
Zhihua Zheng *https://orcid.org/0000-0003-1025-5384*

REFERENCES

1. Bonner R, Albajrami O, Hudspeth J, Upadhyay A. Diabetic kidney disease. Prim Care 2020;47:645-59.
2. Cheng HT, Xu X, Lim PS, Hung KY. Worldwide epidemiology of diabetes-related end-stage renal disease, 2000-2015. Diabetes Care 2021;44:89-97.
3. Levin A, Tonelli M, Bonventre J, Coresh J, Donner JA, Fogo AB, et al. Global kidney health 2017 and beyond: a roadmap for closing gaps in care, research, and policy. Lancet 2017;390:1888-917.
4. Mou Y, Wang J, Wu J, He D, Zhang C, Duan C, et al. Ferroptosis, a new form of cell death: opportunities and challenges in cancer. J Hematol Oncol 2019;12:34.

5. Tang S, Xiao X. Ferroptosis and kidney diseases. Int Urol Nephrol 2020;52:497-503.
6. Weiland A, Wang Y, Wu W, Lan X, Han X, Li Q, et al. Ferroptosis and its role in diverse brain diseases. Mol Neurobiol 2019;56:4880-93.
7. Dixon SJ, Lemberg KM, Lamprecht MR, Skouta R, Zaitsev EM, Gleason CE, et al. Ferroptosis: an iron-dependent form of nonapoptotic cell death. Cell 2012;149:1060-72.
8. Li J, Cao F, Yin HL, Huang ZJ, Lin ZT, Mao N, et al. Ferroptosis: past, present and future. Cell Death Dis 2020;11:88.
9. Hu W, Liang K, Zhu H, Zhao C, Hu H, Yin S. Ferroptosis and its role in chronic diseases. Cells 2022;11:2040.
10. Yang WS, Stockwell BR. Ferroptosis: death by lipid peroxidation. Trends Cell Biol 2016;26:165-76.
11. Ayala A, Munoz MF, Arguelles S. Lipid peroxidation: production, metabolism, and signaling mechanisms of malondialdehyde and 4-hydroxy-2-nonenal. Oxid Med Cell Longev 2014;2014:360438.
12. Ursini F, Maiorino M. Lipid peroxidation and ferroptosis: the role of GSH and GPx4. Free Radic Biol Med 2020;152:175-85.
13. Wang Y, Qiu S, Wang H, Cui J, Tian X, Miao Y, et al. Transcriptional repression of ferritin light chain increases ferroptosis sensitivity in lung adenocarcinoma. Front Cell Dev Biol 2021;9:719187.
14. He J, Li Z, Xia P, Shi A, FuChen X, Zhang J, et al. Ferroptosis and ferritinophagy in diabetes complications. Mol Metab 2022;60:101470.
15. Thevenod F, Wolff NA. Iron transport in the kidney: implications for physiology and cadmium nephrotoxicity. Metallomics 2016;8:17-42.
16. Agborbesong E, Li LX, Li L, Li X. Molecular mechanisms of epigenetic regulation, inflammation, and cell death in ADPKD. Front Mol Biosci 2022;9:922428.
17. Li S, Zheng L, Zhang J, Liu X, Wu Z. Inhibition of ferroptosis by up-regulating Nrf2 delayed the progression of diabetic nephropathy. Free Radic Biol Med 2021;162:435-49.
18. Jiang X, Stockwell BR, Conrad M. Ferroptosis: mechanisms, biology and role in disease. Nat Rev Mol Cell Biol 2021;22:266-82.
19. Zheng J, Conrad M. The metabolic underpinnings of ferroptosis. Cell Metab 2020;32:920-37.
20. Lee JY, Kim WK, Bae KH, Lee SC, Lee EW. Lipid metabolism and ferroptosis. Biology (Basel) 2021;10:184.
21. Lin Z, Liu J, Kang R, Yang M, Tang D. Lipid metabolism in ferroptosis. Adv Biol (Weinh) 2021;5:e2100396.
22. Miess H, Dankworth B, Gouw AM, Rosenfeldt M, Schmitz W, Jiang M, et al. The glutathione redox system is essential to prevent ferroptosis caused by impaired lipid metabolism in clear cell renal cell carcinoma. Oncogene 2018;37:5435-50.
23. Chen X, Li J, Kang R, Klionsky DJ, Tang D. Ferroptosis: machinery and regulation. Autophagy 2021;17:2054-81.
24. Opazo-Rios L, Mas S, Marin-Royo G, Mezzano S, Gomez-Guerrero C, Moreno JA, et al. Lipotoxicity and diabetic nephropathy: novel mechanistic insights and therapeutic opportunities. Int J Mol Sci 2020;21:2632.
25. Russo GT, De Cosmo S, Viazzi F, Pacilli A, Ceriello A, Genovese S, et al. Plasma triglycerides and HDL-C levels predict the development of diabetic kidney disease in subjects with type 2 diabetes: the AMD Annals Initiative. Diabetes Care 2016;39:2278-87.
26. Herman-Edelstein M, Scherzer P, Tobar A, Levi M, Gafter U. Altered renal lipid metabolism and renal lipid accumulation in human diabetic nephropathy. J Lipid Res 2014;55:561-72.
27. Saudek CD, Eder HA. Lipid metabolism in diabetes mellitus. Am J Med 1979;66:843-52.
28. Li H, Xiao Y, Tang L, Zhong F, Huang G, Xu JM, et al. Adipocyte fatty acid-binding protein promotes palmitate-induced mitochondrial dysfunction and apoptosis in macrophages. Front Immunol 2018;9:81.
29. Li HL, Wu X, Xu A, Hoo RL. A-FABP in metabolic diseases and the therapeutic implications: an update. Int J Mol Sci 2021;22:9386.
30. Shi M, Ma L, Fu P. Role of fatty acid binding protein 4 (FABP4) in kidney disease. Curr Med Chem 2020;27:3657-64.
31. Chen Y, Dai Y, Song K, Huang Y, Zhang L, Zhang C, et al. Pre-emptive pharmacological inhibition of fatty acid-binding protein 4 attenuates kidney fibrosis by reprogramming tubular lipid metabolism. Cell Death Dis 2021;12:572.
32. Tanaka M, Furuhashi M, Okazaki Y, Mita T, Fuseya T, Ohno K, et al. Ectopic expression of fatty acid-binding protein 4 in the glomerulus is associated with proteinuria and renal dysfunction. Nephron Clin Pract 2014;128:345-51.
33. Hotamisligil GS, Bernlohr DA. Metabolic functions of FABPs: mechanisms and therapeutic implications. Nat Rev Endocrinol 2015;11:592-605.
34. Ni X, Gu Y, Yu H, Wang S, Chen Y, Wang X, et al. Serum adipocyte fatty acid-binding protein 4 levels are independently associated with radioisotope glomerular filtration rate in type 2 diabetic patients with early diabetic nephropathy. Biomed Res Int 2018;2018:4578140.

35. Lee CH, Cheung CY, Woo YC, Lui DT, Yuen MM, Fong CH, et al. Prospective associations of circulating adipocyte fatty acid-binding protein levels with risks of renal outcomes and mortality in type 2 diabetes. Diabetologia 2019;62:169-77.
36. Fan X, Xu M, Ren Q, Fan Y, Liu B, Chen J, et al. Downregulation of fatty acid binding protein 4 alleviates lipid peroxidation and oxidative stress in diabetic retinopathy by regulating peroxisome proliferator-activated receptor γ-mediated ferroptosis. Bioengineered 2022;13:10540-51.
37. Liu J, Huang R, Li X, Guo F, Li L, Zeng X, et al. Genetic inhibition of FABP4 attenuated endoplasmic reticulum stress and mitochondrial dysfunction in rhabdomyolysis-induced acute kidney injury. Life Sci 2021;268:119023.
38. Luis G, Godfroid A, Nishiumi S, Cimino J, Blacher S, Maquoi E, et al. Tumor resistance to ferroptosis driven by stearoyl-CoA desaturase-1 (SCD1) in cancer cells and fatty acid biding protein-4 (FABP4) in tumor microenvironment promote tumor recurrence. Redox Biol 2021;43:102006.
39. Fang X, Ardehali H, Min J, Wang F. The molecular and metabolic landscape of iron and ferroptosis in cardiovascular disease. Nat Rev Cardiol 2023;20:7-23.
40. Chen X, Kang R, Kroemer G, Tang D. Broadening horizons: the role of ferroptosis in cancer. Nat Rev Clin Oncol 2021;18:280-96.
41. Stockwell BR. Ferroptosis turns 10: emerging mechanisms, physiological functions, and therapeutic applications. Cell 2022;185:2401-21.
42. Liang D, Minikes AM, Jiang X. Ferroptosis at the intersection of lipid metabolism and cellular signaling. Mol Cell 2022;82:2215-27.
43. Yang WS, Kim KJ, Gaschler MM, Patel M, Shchepinov MS, Stockwell BR. Peroxidation of polyunsaturated fatty acids by lipoxygenases drives ferroptosis. Proc Natl Acad Sci U S A 2016;113:E4966-75.
44. Magtanong L, Ko PJ, To M, Cao JY, Forcina GC, Tarangelo A, et al. Exogenous monounsaturated fatty acids promote a ferroptosis-resistant cell state. Cell Chem Biol 2019;26:420-32.
45. Lee H, Zandkarimi F, Zhang Y, Meena JK, Kim J, Zhuang L, et al. Energy-stress-mediated AMPK activation inhibits ferroptosis. Nat Cell Biol 2020;22:225-34.
46. Juszczak F, Caron N, Mathew AV, Decleves AE. Critical role for AMPK in metabolic disease-induced chronic kidney disease. Int J Mol Sci 2020;21:7994.
47. Entezari M, Hashemi D, Taheriazam A, Zabolian A, Mohammadi S, Fakhri F, et al. AMPK signaling in diabetes mellitus, insulin resistance and diabetic complications: a pre-clinical and clinical investigation. Biomed Pharmacother 2022;146:112563.
48. Gewin LS. Sugar or fat?: renal tubular metabolism reviewed in health and disease. Nutrients 2021;13:1580.
49. Thongnak L, Pongchaidecha A, Lungkaphin A. Renal lipid metabolism and lipotoxicity in diabetes. Am J Med Sci 2020;359:84-99.
50. Stadler K, Goldberg IJ, Susztak K. The evolving understanding of the contribution of lipid metabolism to diabetic kidney disease. Curr Diab Rep 2015;15:40.
51. Miguel V, Tituana J, Herrero JI, Herrero L, Serra D, Cuevas P, et al. Renal tubule Cpt1a overexpression protects from kidney fibrosis by restoring mitochondrial homeostasis. J Clin Invest 2021;131:e140695.
52. Shen Y, Chen W, Han L, Bian Q, Fan J, Cao Z, et al. VEGF-B antibody and interleukin-22 fusion protein ameliorates diabetic nephropathy through inhibiting lipid accumulation and inflammatory responses. Acta Pharm Sin B 2021;11:127-42.
53. Fu Y, Sun Y, Wang M, Hou Y, Huang W, Zhou D, et al. Elevation of JAML promotes diabetic kidney disease by modulating podocyte lipid metabolism. Cell Metab 2020;32:1052-62.
54. Mori Y, Ajay AK, Chang JH, Mou S, Zhao H, Kishi S, et al. KIM-1 mediates fatty acid uptake by renal tubular cells to promote progressive diabetic kidney disease. Cell Metab 2021;33:1042-61.